Article

SOURCE DATA | TRANSPARENT PROCESS | OPEN ACCESS

THE EMBO JOURNAL

Rap1 prevents fusions between long telomeres in fission yeast

Lili Pan[1], Duncan Tormey[2,†], Nadine Bobon[1] & Peter Baumann[1,3,*]

Abstract

The conserved Rap1 protein is part of the shelterin complex that plays critical roles in chromosome end protection and telomere length regulation. Previous studies have addressed how fission yeast Rap1 contributes to telomere length maintenance, but the mechanism by which the protein inhibits end fusions has remained elusive. Here, we use a mutagenesis screen in combination with high-throughput sequencing to identify several amino acid positions in Rap1 that have key roles in end protection. Interestingly, mutations at these sites render cells susceptible to genome instability in a conditional manner, whereby longer telomeres are prone to undergoing end fusions, while telomeres within the normal length range are sufficiently protected. The protection of long telomeres is in part dependent on their nuclear envelope attachment mediated by the Rap1–Bqt4 interaction. Our data demonstrate that long telomeres represent a challenge for the maintenance of genome integrity, thereby providing an explanation for species-specific upper limits on telomere length.

Keywords end fusions; fission yeast; genome instability; Rap1; telomere length

DOI 10.15252/embj.2021110458 | Received 15 December 2021 | Revised 4 August 2022 | Accepted 8 August 2022 | Published online 5 September 2022

The EMBO Journal (2022) 41: e110458

Introduction

Telomeres, the structures found at the ends of linear chromosomes, are critical for the maintenance of genome integrity. The leading strand of telomeric DNA is comprised of short G-rich repeats synthesized by the specialized reverse transcriptase telomerase (Pfeiffer & Lingner, 2013). While telomerase solves the end replication problem, telomeres also must be distinguished from DNA double-strand breaks. Defects in chromosome end protection results in the activation of a DNA damage response (DDR), which triggers illegitimate repair events including resection and chromosome end-to-end fusions (de Lange, 2018). Fused chromosomes lead to genomic instability through breakage-fusion-bridge cycles and more immediate, massive rearrangements called chromothripsis (Maciejowski *et al*, 2015). To avoid such catastrophic events, telomeric DNA is bound by several proteins collectively referred to as the shelterin complex, which protects telomeres from unwarranted repair events (de Lange, 2018).

In the fission yeast *Schizosaccharomyces pombe*, a complex comprised of five proteins is at the heart of telomere protection: Taz1 binds double-stranded telomeric repeats and recruits Rap1 (Cooper *et al*, 1997; Chikashige & Hiraoka, 2001; Kanoh & Ishikawa, 2001); whereas Pot1, in complex with Tpz1, binds the single-stranded 3′ overhangs (Baumann & Cech, 2001; Miyoshi *et al*, 2008). These two subcomplexes are bridged by Poz1 (Miyoshi *et al*, 2008). An orthologous molecular bridge, connecting the double-stranded and single-stranded parts of telomeres, is formed by the TIN2 protein in mammalian cells, where the subcomplexes on double-stranded DNA (TRF1, TRF2, RAP1) and single-stranded overhangs (POT1 and TPP1) also share fundamental similarities with their fission yeast counterparts (Zhong *et al*, 1992; Chong *et al*, 1995; Bilaud *et al*, 1997; Broccoli *et al*, 1997; Kim *et al*, 1999; Li *et al*, 2000; Baumann & Cech, 2001; Houghtaling *et al*, 2004; Liu *et al*, 2004; Ye *et al*, 2004). Deletion of *taz1*, *rap1*, or *poz1* in *S. pombe* results in massive telomere elongation, suggesting a role of these factors in inhibiting telomerase (Cooper *et al*, 1997; Chikashige & Hiraoka, 2001; Kanoh & Ishikawa, 2001; Miyoshi *et al*, 2008). Deletion of *taz1* and *rap1* also causes chromosome end-to-end fusions when cells are arrested in G1, supporting a direct role of these factors in end protection (Ferreira & Cooper, 2001; Miller *et al*, 2005). Our previous analysis of Rap1 and Poz1 revealed that their function in telomere length regulation is limited to forming part of a molecular bridge connecting the double- and single-stranded parts of the telomeres and that the proteins can be entirely replaced by a short covalent linker between Tpz1 and Taz1 (Pan *et al*, 2015). While such a "mini-shelterin" restores wildtype telomere length, chromosome ends are still vulnerable to undergoing fusions via illegitimate repair events when Rap1, but not Poz1, is absent. Adding back Rap1 restored full protection, indicating that Rap1 prevents end fusions independent of its role as a molecular bridge between Taz1 and Poz1. A function for Rap1 in inhibiting fusions is highly conserved as shown by related findings in budding yeast and human cells (Pardo & Marcand, 2005; Bae & Baumann, 2007; Sarthy

1 Department of Biology, Johannes Gutenberg University, Mainz, Germany
2 Stowers Institute for Medical Research, Kansas City, MO, USA
3 Institute of Molecular Biology, Mainz, Germany
*Corresponding author. Tel: +49 6131 39 21422; E-mail: peter@baumannlab.org
†Present address: Synthego, Bend, OR, USA

et al, 2009). At least in human cells, protection by Rap1 is redundant with other protective mechanisms and is only observed when TRF2 is absent or telomeres are critically short (Sarthy *et al*, 2009; Sfeir *et al*, 2010; Lototska *et al*, 2020).

The N-terminal half of fission yeast Rap1 contains three domains, a BRCA1 C-terminal (BRCT), a Myb- and a Myb-Like domain (Chikashige & Hiraoka, 2001; Kanoh & Ishikawa, 2001). The C-terminal half harbors a Poz1 interaction domain (PI domain, Pan *et al*, 2015) and a structurally conserved Rap1 C-terminus (RCT), which interacts with Taz1 in *S. pombe*, TRF2 in human, and Sir3 in *S. cerevisiae*, respectively (Moretti *et al*, 1994; Li *et al*, 2000; Chen *et al*, 2011). The PI and RCT domains are separated by a mostly unstructured region of approximately 150 amino acids. In this study, we combined a deletion scan and random mutagenesis screen to identify elements in Rap1 that are critical for preventing telomere fusions. Analysis of the mutagenesis screen by next-generation sequencing identified several amino acid positions in the region between PI and RCT domains that are important for end protection. Intriguingly, mutations at these positions specifically rendered elongated telomeres susceptible to end fusions, whereas telomeres of wildtype length remained protected in the mutants. Contrary to the conventional thinking that only critically short telomeres are at risk of being mistaken for DNA breaks, our data suggest that under certain conditions long telomeres can also be susceptible to uncapping and thus become a source of genomic instability. These observations provide a conceptional framework for why cells maintain telomeres within a clearly defined size range and why overly long telomeres may undergo rapid deletion events (Li & Lustig, 1996).

Results

The region between PI and RCT domains is important for inhibiting end fusions

To test which part of Rap1 is required for end protection, we created a series of Rap1 domain deletions (Fig 1A). Chromosome end fusions were examined by pulsed-field gel electrophoresis of NotI-digested genomic DNA followed by Southern blotting with probes specific for the chromosome terminal fragments C, I, L, and M (Fig 1B). Constructs lacking the BRCT, Myb or Myb-L domain was found to retain the ability of the wildtype protein to prevent end fusions (Fig 1C, lanes 2–4). The ΔPI mutant was previously shown to have elongated telomeres due to the disruption of the interaction between Rap1 and Poz1 (Pan *et al*, 2015). Despite the long telomere phenotype, the ΔPI mutant was proficient at preventing end fusions (lane 5), consistent with previous results that Poz1 is not required for end protection (Fujita *et al*, 2012b; Pan *et al*, 2015). Among the deletion mutants tested here, only Rap1ΔRCT displayed a chromosome end fusion phenotype (lane 6), consistent with the role of the RCT domain in mediating the interaction with Taz1 and thus being responsible for the recruitment of Rap1 to telomeres (Chen *et al*, 2011). The less severe fusion phenotype observed in the ΔRCT mutant compared with *rap1*Δ (compare lanes 6 and 7) may be due to residual recruitment of Rap1ΔRCT to telomeres through the interaction with Poz1.

To further characterize the requirements for end protection, we introduced N-terminal deletions of increasing size. A fragment comprising amino acids 440–693 was sufficient to prevent end fusions (Fig 1D, lane 4), confirming previously reported results (Fujita *et al*, 2012b). By contrast, the expression of amino acids 513–693 or a shorter fragment failed to prevent end fusions similar to *rap1*Δ (lanes 6 and 7, Fujita *et al*, 2012b). Amino acids 491–693 displayed a weaker fusion phenotype. This was surprising as the fragment only lacks the PI domain relative to 440–693 and *rap1*ΔPI did not show a fusion phenotype (compare lanes 5 in Fig 1C and D). Possible explanations for this observation are that the truncation of amino acids 1–490 affects the folding of the remaining protein sequence and/or differences in the protein expression levels. Indeed, western analysis of C-terminally V5 epitope-tagged Rap1 showed substantially lower protein levels for Rap1_491–693 compared with full-length Rap1 or Rap1_440–693 (Appendix Fig S1). It must be noted, however, that Rap1_440–693 level is also substantially lower than full-length Rap1, yet this deletion mutant is fully functional in the same background and under the same growth conditions.

To further investigate a possible role for the PI domain in end protection, we next fused Rap1_491–693 to the C-terminus of Poz1 and integrated this construct at the endogenous *poz1* locus in cells, which possess elongated telomeres due to the absence of Rap1 in the starting strain. The fusion protein is expressed at lower than wildtype but higher than Rap1_440–693 levels (Appendix Fig S1). Over the course of 14 successive restreaks on agar plates (approximately 310 generations), telomere length decreased and stabilized at slightly shorter than wildtype length (Fig 2A). Interestingly, at the 5th restreak (approximately 110 generations), cells characterized by intermediate telomere length showed mild end fusions, whereas no fusion phenotype was observed after 14 restreaks when telomeres are no longer elongated (Fig 2B, compare lanes 3 and 4). These results confirm the dispensability of the PI domain under certain conditions but, more importantly, suggest that telomere length directly affects the degree of end protection with longer telomeres being more likely to fuse than those of normal length.

To test whether the RCT domain itself is directly contributing to end protection beyond its function in the recruitment of Rap1 to telomeres, we fused Rap1ΔRCT to Taz1. This fusion protein rescued both the telomere elongation and end fusion phenotypes caused by the lack of the RCT domain (Fig 2C, lanes 2–5 and D, lane 2). By contrast, fusing Rap1ΔRCT to Poz1 neither rescued telomere length nor end protection (Fig 2C, lanes 6–9 and D, lane 3). These results support that the PI and RCT domains are not directly involved in the protective role of Rap1 in end protection. They are needed for the recruitment and stabilization of the protein but can each be replaced by covalent linkers to provide tethers to Poz1 and Taz1, respectively.

Mutagenesis screen identifies residues important for end protection

As the results described above pointed to a function of the region between PI and RCT domains in end protection, we generated a library of randomly mutagenized Rap1_440–693 fragments and introduced them into *rap1*Δ cells (Fig 3A). The average mutation rate was 0.785% per nucleotide position as determined by Illumina sequencing of the library prior to introduction into *S. pombe*. We reasoned that cells harboring Rap1 mutations that impair end

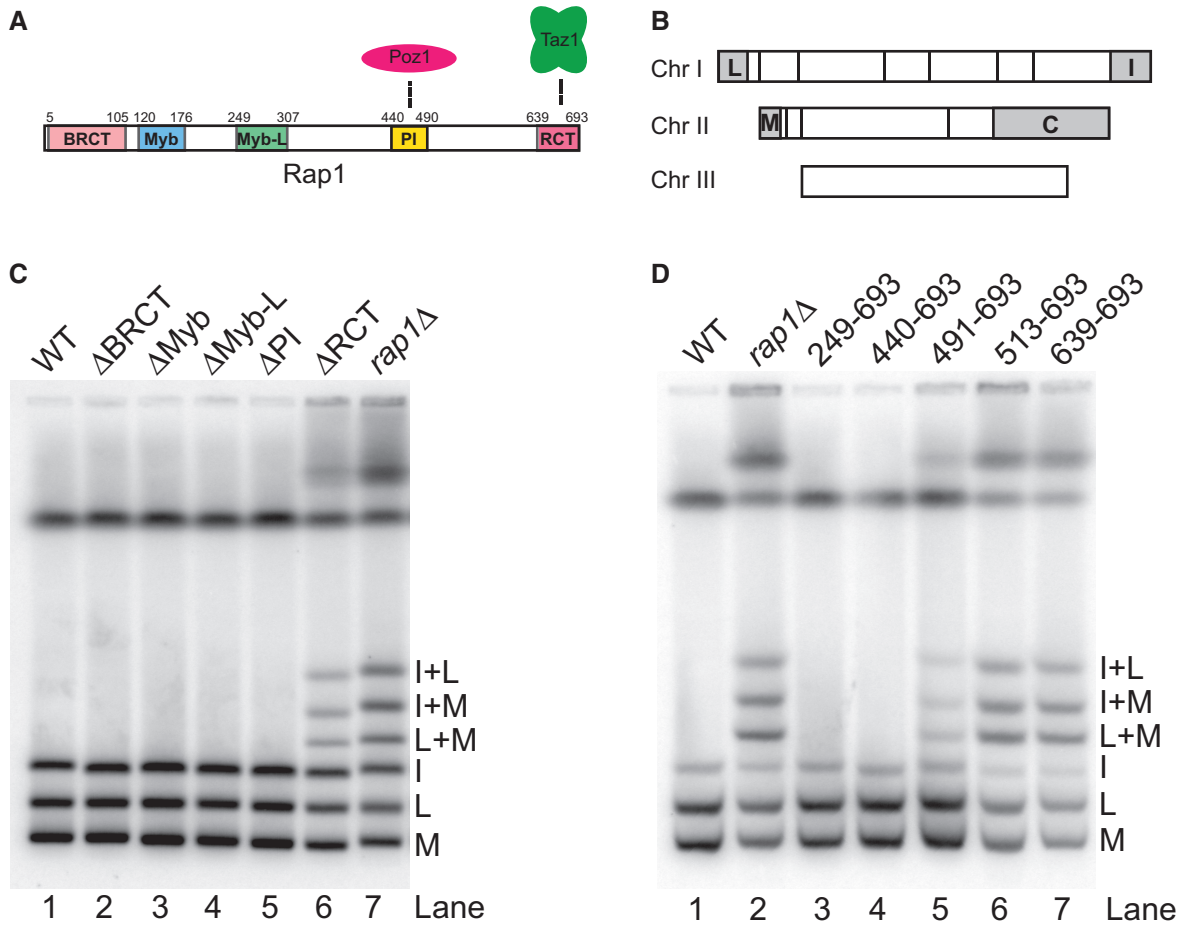

Figure 1. The C-terminal amino acids 440–693 of Rap1 are sufficient to protect telomeres against end fusions.

A Schematic representation of Rap1 domain structure.

B Schematic of NotI digestion fragments of *S. pombe* chromosomes. The terminal fragments of chromosome I are named L and I; those of chromosome II M and C. Chromosome III lacks NotI restriction sites.

C End fusion analysis for domain deletion mutants of Rap1. NotI-digested genomic DNA from nitrogen-starved cells was analyzed by pulsed-field gel electrophoresis (PFGE) and Southern blot with probes specific for the terminal C, I, L, and M fragments from chromosomes I and II.

D PFGE analysis as in (C) for nitrogen-starved cells harboring N-terminal truncation mutants of Rap1. All mutants were V5-tagged at their C-terminus.

protection would be delayed in resuming cell division following G1 arrest, as chromosome end fusions occurring during G1 arrest will delay or prevent re-entry into the cell cycle. Hence, point mutations in Rap1 that affect its end protection function are expected to decrease in abundance over multiple rounds of arrest and return to growth (Fig 3A). After each round, cells were collected to assess telomere length and prevalence of end fusions. The average telomere length and incidence of end fusions declined over the course of five rounds of arrest and returned to growth as expected for a selection experiment (Fig EV1).

We then utilized Illumina sequencing to assess changes in the prevalence of alternative nucleotides at each position over time. An 877 bp fragment including Rap1_440–693 and short flanking regions was amplified from each round of the time course performed in triplicate. The mutation frequency profiles were similar before and approximately 12 generations after transformation into *S. pombe* confirming the preservation of library complexity upon transformation (Appendix Fig S2). After five rounds of G1 arrest followed by a return to growth, the three replicates displayed striking overlap in which nucleotide positions showed a decrease in nucleotide substitution and which ones did not (Appendix Fig S3A). Confirming that the observed changes were indeed the result of selection at the protein level during growth in culture, the incidence of the alternative nucleotides decreasing over time was limited to codon positions 1 and 2, while position 3 nucleotides were not under selection (Appendix Fig S3B).

Applying a filter to identify those positions where alternative nucleotides consistently decreased each round in each of the replicates over the course of five rounds, we identified 20 nucleotide positions (Fig 3B), corresponding to 17 amino acids (Fig 3C), for which the native nucleotide was under strong selection. For three amino acids, two codon positions were affected (Fig 3C and Appendix Table S1). In all cases, the alternative nucleotides that were selected against changed the encoded amino acid. After five rounds of arrest and return to growth, all except one position showed a greater than 2-fold change in favor of the native

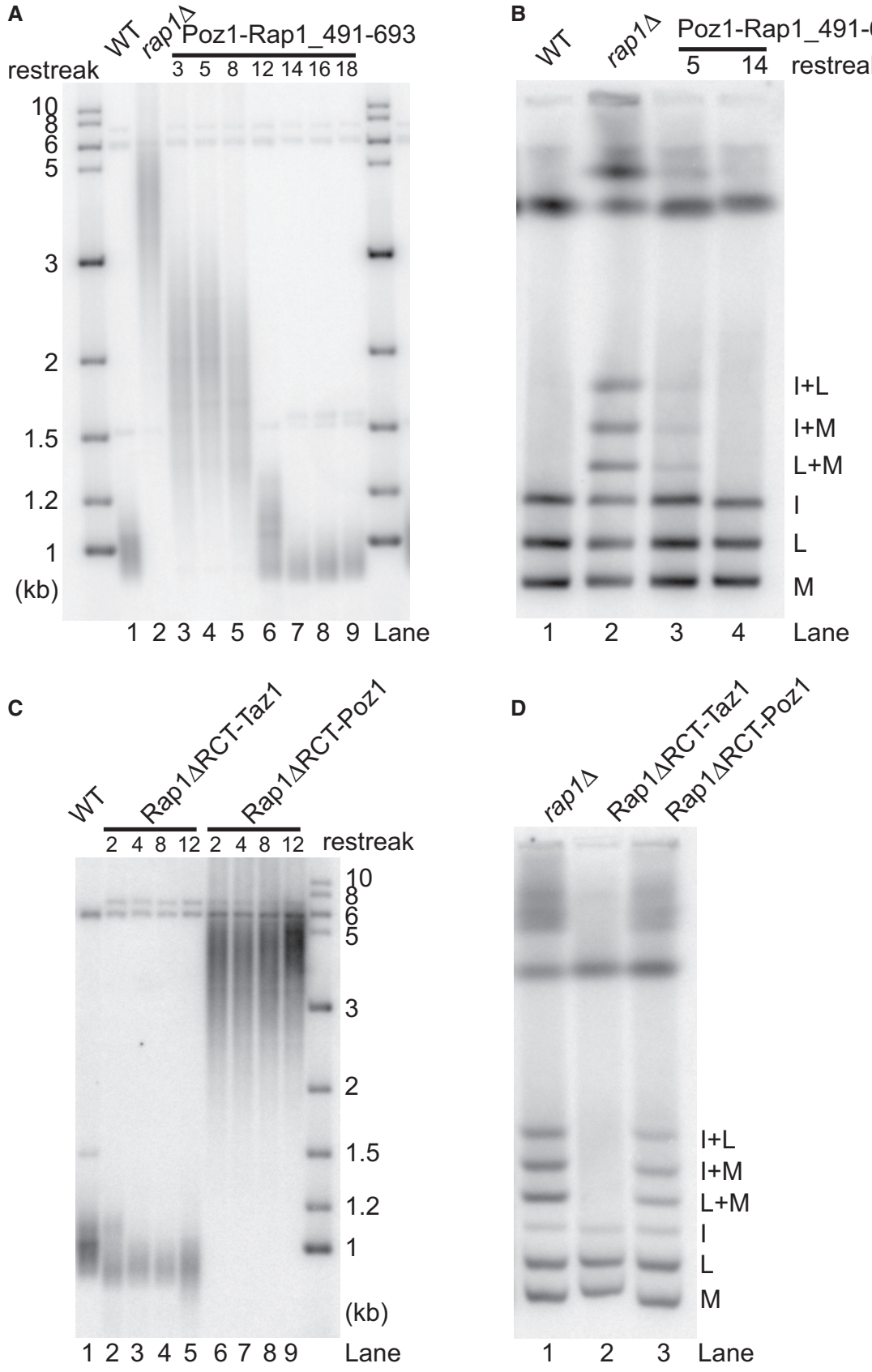

Figure 2.

Figure 2. Covalent linkers can replace the PI and RCT domains of Rap1.

A Telomere length analysis of cells from different sequential restreaks following the introduction of Poz1-V5-Rap1_491–693 into *rap1*Δ cells. Telomere length was assessed by Southern blotting of EcoRI-digested genomic DNA probed with a telomere-specific probe.

B PFGE analysis of nitrogen-starved Poz1-V5-Rap1_491–693 cells after 5 and 14 restreaks.

C Telomere length analysis of cells with Rap1ΔRCT fused to Taz1 or Poz1 with intervening V5 tag. The fusion protein was integrated at the endogenous *rap1* locus in the context of *taz1*Δ or *poz1*Δ, respectively. Different sequential restreaks following the introduction of the fusion construct were analyzed.

D PFGE analysis for nitrogen-starved Rap1ΔRCT-V5-Taz1 and Rap1ΔRCT-V5-Poz1 from 2nd restreak.

nucleotide (Fig 3C). In aggregate, these results confirmed the robustness of the assay and suggested that the identified amino acid positions must be important for end protection.

Characterization of the identified amino acid positions

Of the positions identified in this screen, 10 clustered within the RCT domain (between amino acid 639 and 693) and 7 were found between positions 491 and 638 (Fig 4A). No positions within the PI domain were under selection, further confirming that this region is dispensable for the protection of telomeres from end joining. By contrast, mutations in the RCT domain are expected to disrupt the recruitment of Rap1 to telomeres. Indeed, several positions under selection make contact with Taz1 in the nuclear magnetic resonance structure (Chen *et al*, 2011), and we considered these positions as validation of the screen and did not further investigate the effect of the individual mutations in this region. Alignment of *S. pombe* Rap1 with two other fission yeast species, *S. octosporus* and *S. cryophilus*, showed that 5 of the 7 amino acids in the 491–638 region are identical in all three species and one represents a conserved valine to isoleucine change (Fig 4A). Interestingly, 6 of the 7 amino acids are within a 13 amino acid stretch (499–511) which at the time of the analysis was uncharacterized and we referred to as the protection patch or p-patch for short.

To confirm the importance of the identified positions, we created plasmids carrying the mutations A502W, F503L, Q506R, V507G, Y511N, and F545L, and introduced them into *rap1*Δ cells to assess whether protection from end fusions was compromised (Fig 4B and C). In addition, a compound mutant containing the 6 amino acids located within the p-patch was generated and is referred to as M6. Finally, all 7 positions identified to be under selection outside the RCT domain were combined in one construct (M7). As controls, we selected two amino acid changes in the RCT domain, I655F and S664L. I655 is part of the hydrophobic groove that interacts with Taz1 (Chen *et al*, 2011) and mutations of S664 were selected against most strongly of all the identified positions (Fig 3C). After recovery from transformation, cells were subjected to G1 arrest (Restreak 0) and analyzed by pulsed-field gel electrophoresis (PFGE; Fig 4B). The two mutations in the RCT domain, I655F and S664L, behaved as null alleles showing similar levels of fusions as the empty vector control (Fig 4B, lanes 9–11 and D). The mutations in the p-patch and F545 displayed an intermediate level of fusions (Fig 4B, lanes 1–8 and D). Interestingly, the wildtype C-terminal fragment of Rap1 also displayed fusions, albeit at lower levels than the point mutants (Fig 4B, lane 12 and D). These results confirmed that changes in Illumina sequencing read counts attributed to specific nucleotide changes are indeed a reflection of growth differences caused by varying levels of end fusions in the competition experiment.

To assess whether telomere length affected the incidence of end fusions, the cells carrying the 440–693 WT or mutant fragments were restreaked five times on plates (approximately 110 generations). In comparison to the cells analyzed immediately after transformation (Restreak 0), fusions were reduced by more than two-fold for the WT fragment, whereas fusions remained high in the RCT mutants I655F and S664L and the empty vector (Fig 4C, lanes 9–12 and D). Strikingly, all individual and combined mutants in the p-patch and F545 showed decreased levels of fusions in Restreak 5 compared with Restreak 0 (Fig 4C, lanes 1–8 and D). Examination of telomere length revealed that Restreak 0 samples had long and heterogenous telomeres similar to *rap1*Δ cells (Appendix Fig S4A). By contrast, over the course of five restreaks telomeres had shortened substantially for the strains harboring WT, p-patch, and F545 mutants but not for the RCT mutants or empty vector (Appendix Fig S4B). These correlations in telomere length and incidence of end fusions when end protection is compromised strongly support that telomere length affects protection in a manner that makes longer telomeres more susceptible to fusions than shorter ones.

To further test whether the p-patch and F545 are specifically required for the protection of long telomeres, we created four internal deletions within the region between the PI and RCT domains and integrated them into the genome by directly replacing endogenous *rap1*$^+$ (Fig 5A). Western blot analysis showed that the expression levels for WT and all deletion mutants were within 2.5-fold of each other with WT and Δ593–638 at the lower end of this range (Fig 5B). Consistent with previous results that only the Poz1 and Taz1 interaction domains are required for telomere length maintenance (Pan *et al*, 2015), the three nonoverlapping deletion mutants exhibited wildtype telomere length (Fig 5C, lanes 4–6) and no end fusion phenotype (Fig 5D, lanes 3–5). When the entire 491–638 region was deleted, we observed slight telomere elongation (Fig 5C, lane 3) and mild fusions (Fig 5D, lane 6) but only in the presence of the V5 epitope tag (compare Fig 5C, lane 3 and 7; D lane 6 and 7). These results demonstrate that the entire region between the PI and RCT domains is dispensable for end protection if telomeres are wildtype in length. By contrast, when telomeres were elongated by deletion of *poz1*, Rap1Δ491–540, lacking the p-patch, and Rap1Δ541–592, where F545 resides, both displayed end fusion phenotypes (Fig 5E, lanes 3 and 4); whereas Rap1Δ593–638, where no positions had been identified in our screen, showed full protection even in the presence of very long telomeres (lane 5).

Telomere length impacts end protection

To further probe the telomere length dependence of end protection, we integrated the p-patch and F545 mutants in the context of full-

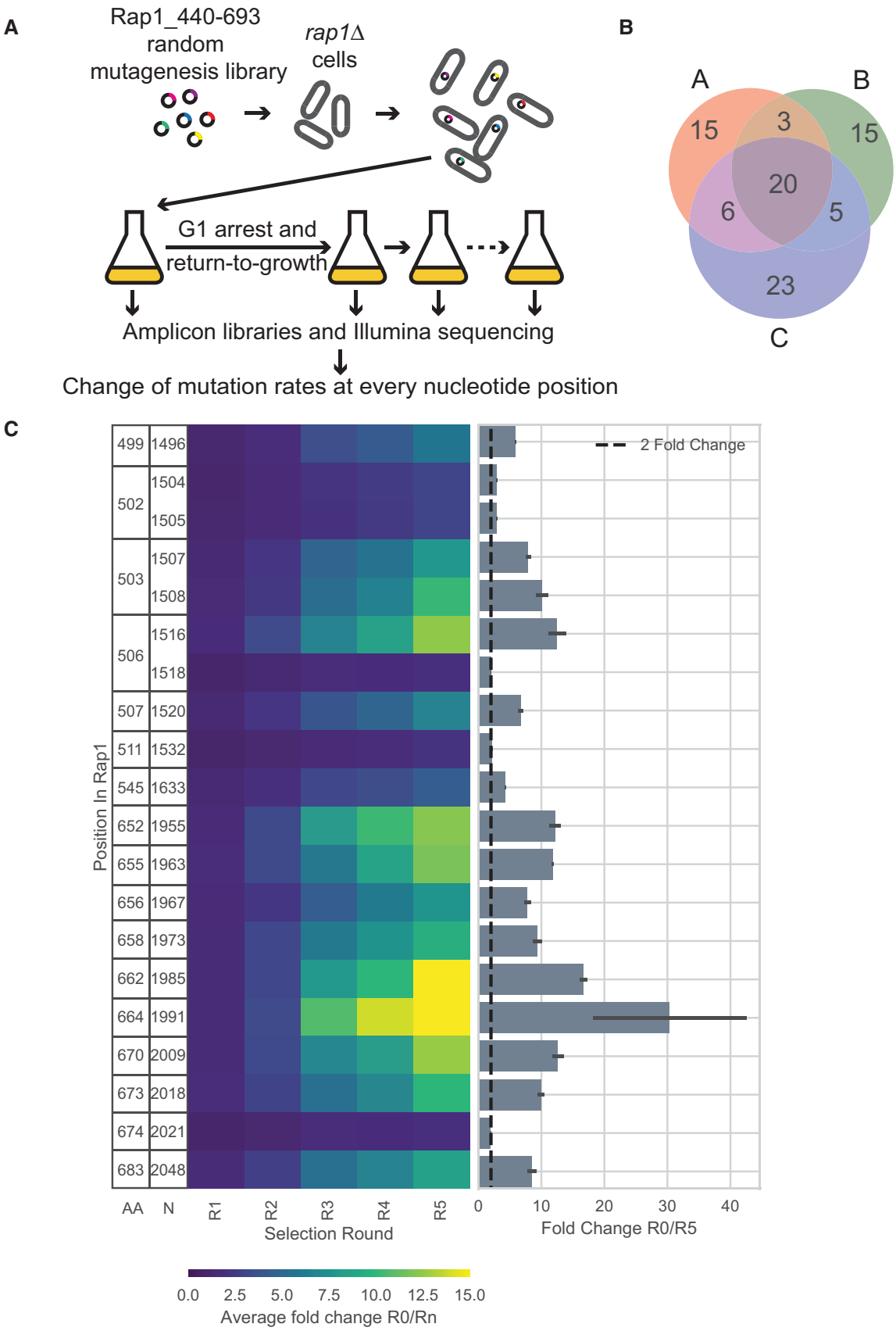

Figure 3.

Figure 3. Random mutagenesis screen and Illumina sequencing identify positions important for end protection.

A Schematic of the mutagenesis screen. A random mutagenesis plasmid library of Rap1_440–693 under the endogenous *rap1* promoter was introduced into *rap1*Δ cells. The cultures were subjected to five rounds of arrest and returned to growth. Amplicon libraries covering the *rap1* fragments were generated and Illumina sequenced. Change of mutation rates at every nucleotide position was calculated.

B Venn diagram of three biological replicates showing the positions where the non-native nucleotides consistently decrease from one round to the next.

C Left panel: heat map showing the average changes in non-native nucleotides after each round of arrest and returned to growth. Numbers represent the amino acid position in the full-length protein (AA, first column) and the nucleotide position in cDNA (N, second column). Columns R1 to R5 represent rounds of selection. The color of the cells represents the average fold change in non-native nucleotides compared with the initial time point R0. Right panel: bar graph depicting average fold change for R5 over R0. Error bars show standard deviation. A dashed line denotes the 2-fold cutoff. $N = 3$, biological replicates.

length *rap1* at the endogenous locus. All mutants were expressed at the same or slightly higher levels than the wildtype protein (Appendix Fig S5A and B). Under these conditions, none of the point mutants displayed chromosome end fusions upon G1 arrest (Fig 6A), consistent with the internal deletion results described above. Even when full-length Rap1 was replaced with the C-terminal fragment in an attempt to create a sensitized background (Appendix Fig S5B), none of the mutations compromised end protection (Fig 6B). As expected, all mutants maintained wildtype telomere length in the context of full-length and the C-terminal fragment (Fig EV2A). Strikingly, as telomeres elongated following the deletion of *poz1* (Fig EV2B), fusions were readily detected in the p-patch (M6) and F545L mutants but not in the presence of wildtype Rap1 (Fig 6C, lanes 2–4). This result cannot be explained by differences in protein levels as the mutants were expressed at slightly higher levels than wildtype Rap1 (Appendix Fig S5C). In the sensitized context of the C-terminal fragment of Rap1 (440–693), even the wildtype sequence was unable to fully protect elongated telomeres (Fig 6C, lane 5). Moreover, combining the expression of only the C-terminal fragment with the point mutations had an additive effect on the level of chromosome end fusions (compare lanes 5 with 6 and 7). No end fusions were observed when the gene encoding ligase IV was deleted, demonstrating that the fusions are indeed mediated by the classical NHEJ pathway (Fig EV3).

To test whether the end fusion phenotype was primarily linked to telomere length or perturbation of the shelterin complex, we also induced telomere elongation by deleting the leucine carboxyl methyltransferase *ppm1* gene. This deletion causes dramatic telomere elongation similar to *poz1*Δ (Fig EV2C; Lorenzi *et al*, 2015), but Ppm1 is not a member of the shelterin complex, and the mechanism by which its deletion causes telomere elongation remains unknown. Deletion of *ppm1* alone or in combination with a N-terminal V5-tagged wildtype *rap1* did not cause end fusions (Fig 6D, lane 2 and 3). However, fusions were detected when combined with the p-patch mutant or F545L (Fig 6D, lanes 4 and 5). Rap1 wildtype and mutant protein levels were not reduced in the absence of *ppm1* (Appendix Fig S5D). This result further confirmed that long telomeres are sensitive to fusions in the context of the newly identified *rap1* alleles.

We next tested whether shorter than wildtype telomeres were also more vulnerable to fusions in the presence of the Rap1 mutations. Deletion of *pof8* impairs telomerase biogenesis, and consequently, *pof8*Δ cells have very short telomeres (Collopy *et al*, 2018; Mennie *et al*, 2018; Paez-Moscoso *et al*, 2018). Telomere length increased slightly when N-terminally V5-tagged wildtype Rap1, M6, or F545L were introduced (Fig EV4A). Protein levels were similar across the strains, with the mutants being expressed at slightly higher levels, consistent with other strain backgrounds (Appendix Fig S5E). While G1-arrested cells with short telomeres carrying untagged or V5-tagged wildtype Rap1 showed no end fusions (Fig EV4B, lanes 5 and 6), fusions were detected in the M6 and F545L mutants (lanes 7 and 8). However, the levels were lower in comparison to cells with long telomeres (comparing lanes 7 and 8 to lanes 3 and 4).

The vulnerability of long telomeres is not due to differences in Rap1-binding or single-stranded overhang length

Neither p-patch nor F545L is within the Taz1- or Poz1-interaction domains, nor are the mutations themselves associated with telomere length changes. Nevertheless, our data up to this point did not address the possibility that telomere association is affected by the mutations. To test this, a chromatin immunoprecipitation (ChIP) experiment followed by quantitative real-time PCR was performed. Wildtype Rap1 and the F545L and M6 mutants precipitated similar levels of telomeric DNA, indicating that reduced occupancy at telomeres is not the reason why the mutations cause a loss of end protection. This was the case, whether telomere length was wildtype (Fig 7A) or longer due to the presence of *poz1*Δ (Fig 7B).

Deletion of *taz1* or *rap1* results in a strong increase in single-stranded telomeric DNA (Miller *et al*, 2005, 2006). We thus wondered whether the Rap1 mutations may revert this effect, which in turn would make telomeres more susceptible to undergoing end fusions by NHEJ. We employed duplex-specific nuclease (DSN) to degrade all double-stranded DNA and directly measure the remaining single-stranded telomeric DNA (Zhao *et al*, 2011). Probing for the G-rich strand, we found that the increase in single-stranded signal associated with *taz1*Δ and *rap1*Δ is also observed in strains deleted for *poz1* or *ppm1* (Fig 7C top panel). However, within the same genetic background, the Rap1 mutations showed the same signal strength as wildtype, arguing against the possibility that the mutations reduce the length of the single-stranded overhang. As expected, no single-stranded signal was detected when probing for the C-rich strand (Fig 7C, lower panel). Although the assay cannot rule out the possibility of small size differences in G-strand overhang length, the signals are indistinguishable both in size and in intensity between wildtype Rap1 and the two Rap1 mutants within each genetic background (WT, *poz1*Δ, and *ppm1*Δ), suggesting that the Rap1 mutations do not cause loss of single-stranded overhang.

Nuclear envelope attachment contributes to the protection of long telomeres

Following our initial characterization of the p-patch mutants, biochemical and structural analyses of the Rap1–Bqt4 interaction was published (Hu *et al*, 2019) and revealed that the p-patch overlaps

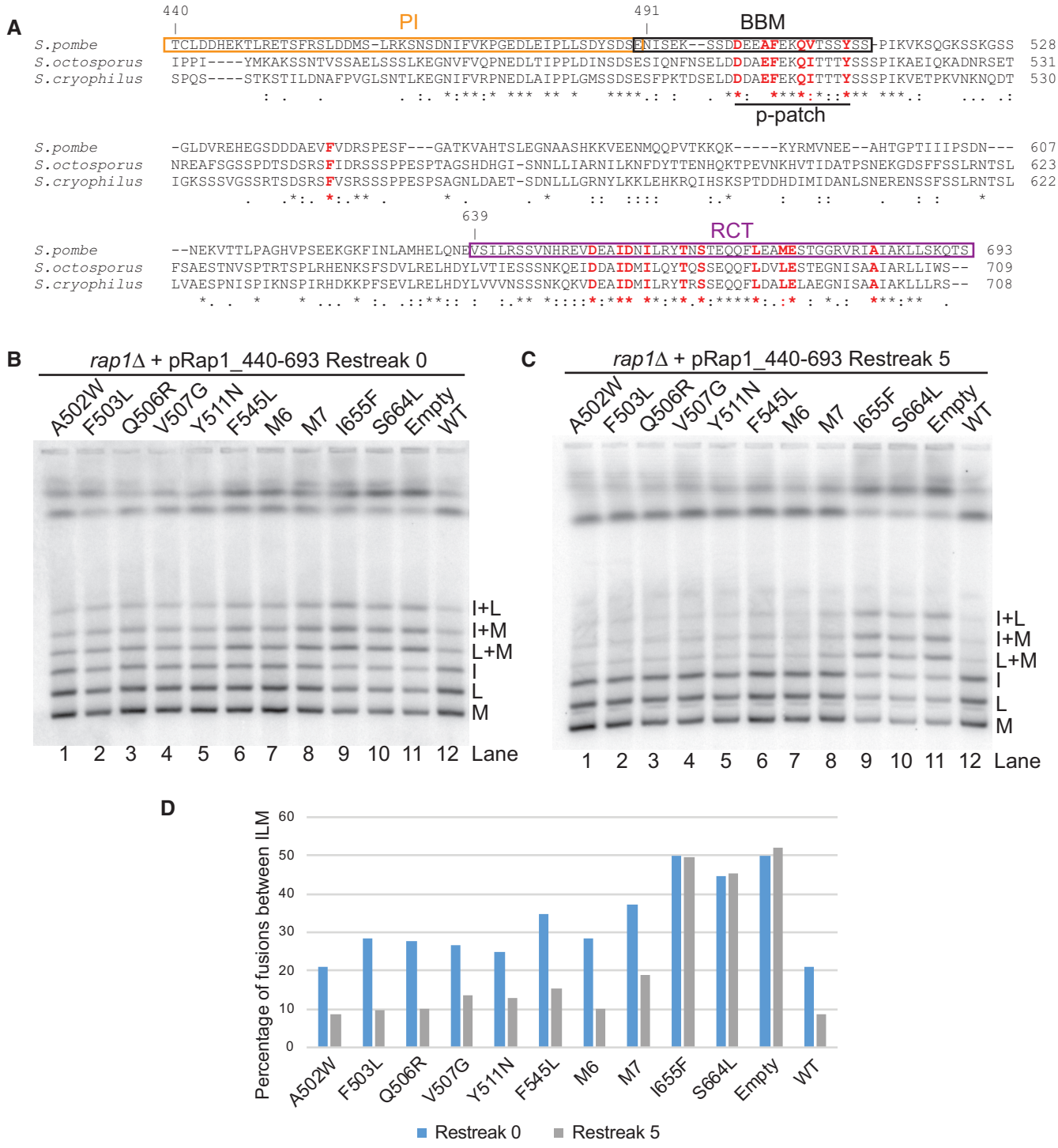

Figure 4. Important amino acids for telomere protection in Rap1_440–693.

A Clustal Omega (1.2.4) alignment of Rap1 protein sequences from *S. pombe*, *S. octosporus*, and *S. cryophilus* (Sievers *et al*, 2011). Amino acids identified in the mutagenesis screen are marked in red. Amino acids 499 to 511 harbored 6 of the selections and the region was named the p-patch. The previously described PI, BBM and RCT domains are shown for reference.

B PFGE analysis of cells containing plasmids of Rap1_440–693 with mutations of the amino acids identified in (A) in the context of *rap1*Δ. Cells were subjected to nitrogen-starvation after recovery from transformation (Restreak 0).

C PFGE analysis of nitrogen-starved cells harboring the same mutations after 5 restreaks on plates (approximately 110 generations).

D Quantification of (B) and (C) using Fiji. The *y*-axis shows the percentage of intensity represented by the three fusion bands (I + L, I + M, and L + M) relative to the total intensity of the fused and unfused signals. WT: wildtype Rap1_440–693.

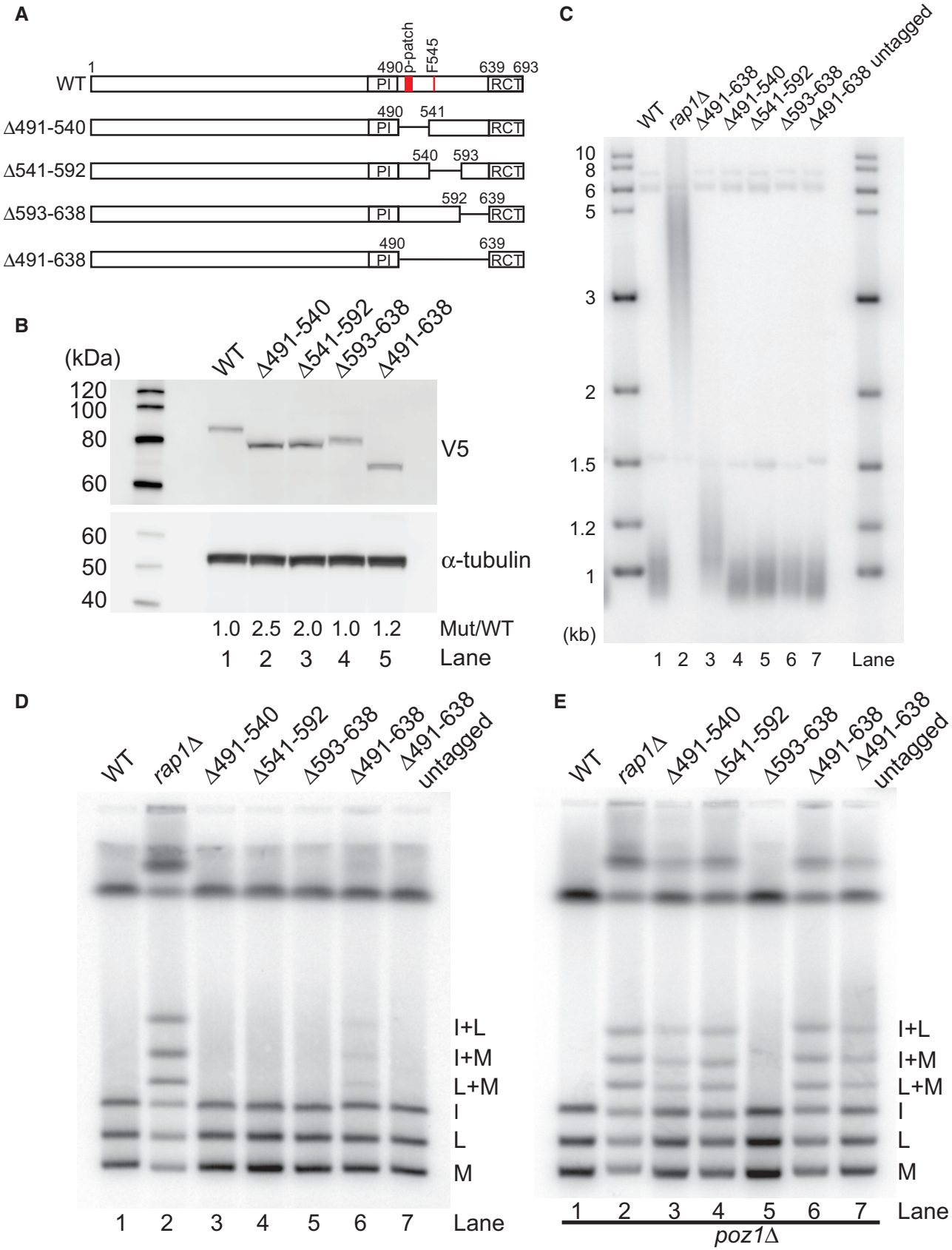

Figure 5.

Figure 5. Δ491–540, Δ541–592 but not Δ593–638 of Rap1 leads to end fusions with elongated telomeres.

A Schematics of the internal deletion mutants between PI and RCT domains.
B Western blot analysis of N-terminally V5-tagged truncation mutants using anti-V5 antibody. Anti-α-tubulin was used as a loading control. Quantification of Rap1 mutant protein levels relative to WT normalized to α-tubulin is shown beneath the gel.
C Telomere length analysis of the mutants by Southern blot with telomere-specific probe. All mutants are V5-tagged except for Δ491–638 untagged (lane 7).
D PFGE analysis of the same strains in (C) that were nitrogen-starved.
E PFGE analysis of nitrogen-starved internal deletion mutants in *poz1*Δ background.

with the Bqt4 binding motif (BBM) of Rap1. The Rap1–Bqt4 interaction tethers telomeres to the nuclear envelope (NE), and is required during meiosis for telomere clustering, meiotic recombination, and spore formation (Chikashige *et al*, 2009; Fujita *et al*, 2012a) but is largely dispensable for the maintenance of telomere length and the silencing of subtelomeric genes during mitotic growth. Considering the overlap of p-patch and BBM, we wondered whether the nuclear envelope attachment of telomeres was important for the protection of long telomeres against fusions. Telomere localization within the nucleus is commonly assessed by mapping telomeric foci to one of three concentric nuclear zones of equal surface area (Hediger *et al*, 2002, Fig 8A). Nup44-mCherry was used to label the NE and Pot1-GFP to visualize telomeres. Consistent with previous results that loss of *bqt4* releases telomeres from the NE (Chikashige *et al*, 2009; Maestroni *et al*, 2020), a significant decrease in the fraction of Pot1-GFP foci was observed in zone I (nuclear periphery) in cells deleted for *bqt4* (Fig 8B). Localization of telomeres in zone I was diminished to the same extent when Rap1 was replaced with the M6 mutant but not with the F545L mutant (Fig 8B). Identical results were obtained when telomeres were visualized with Taz1-GFP (Fig EV5A). In summary, we conclude that the p-patch mutants impair NE attachment presumably by disrupting the Rap1–Bqt4 interaction. Interestingly, the F545L mutant affects end protection in a manner that is independent of the interaction with Bqt4. We further verified the specific loss of interaction using the yeast two-hybrid assay. The M6 mutant compromised the Rap1–Bqt4 interaction while F545L showed wildtype interaction (Fig 8C). Both M6 and F545L mutants interact with Taz1 like wildtype.

To further test to what extent the NE attachment promotes the protection of long telomeres, PFGE was performed with genomic DNA from *bqt4*Δ and *bqt3*Δ cells. Bqt3 also localizes in the inner nuclear membrane and interacts with and protects Bqt4 (Chikashige *et al*, 2009). No end fusions were observed in *bqt4*Δ or *bqt3*Δ cells when telomere length was near wildtype (Fig 8D, lanes 3 and 4). However, when telomeres were elongated by loss of Poz1 (Fig EV5B), fusions were detected in both *bqt4*Δ and *bqt3*Δ cells (Fig 8D, lanes 5 and 6). Rap1 protein levels were similar to wildtype in the deletion mutants (Appendix Fig S5F). The dependence of the fusions on ligase IV confirmed that they are mediated by NHEJ (Fig 8E). In aggregate, these results reveal a role for NE attachment in specifically protecting long telomeres. It is worth noting, however, that the level of fusions in *bqt4*Δ or *bqt3*Δ were lower compared to that in the *rap1* p-patch mutant, suggesting that additional mechanisms are in play. Consistent with this notion, we found that mutation of F545 compromises the protection of long telomeres without affecting NE attachment.

Discussion

Rap1 plays key roles in limiting telomere elongation and protecting chromosome ends from fusions. While its role in regulating telomere length is mainly based on it being part of a protein bridge that tethers the single- and double-stranded parts of the telomere (Pan *et al*, 2015; Kim *et al*, 2017), its contributions to preventing chromosome end fusions are more complex. Using molecular genetic approaches, we have now identified several amino acid positions within Rap1 that are particularly important for the protection of long telomeres. Our results reveal that the requirements for end protection vary depending on the length of a telomere and that one of the mechanisms by which Rap1 protects chromosome ends is by limiting telomere elongation itself. Already elongated telomeres are protected by tethering them to the nuclear periphery, a function that is not required for the protection of shorter telomeres.

Examining end protection in cells with wildtype telomere length revealed surprising flexibility in terms of the required structural elements. Deletions that in aggregate cover the entire protein (Δ1–439, Δ440–490, Δ491–540, Δ541–592, Δ593–638, Δ639–693) showed that any specific region can be deleted or replaced with a simple linker while maintaining the protective function of the protein (Figs 1, 2 and 5). These results demonstrate that any element within Rap1 that is involved in end protection, functions in a redundant manner. Considering the catastrophic consequences that follow failure to protect chromosome ends from undergoing fusions, redundancy is perhaps to be expected. Similarly, Rap1 in budding yeast inhibits NHEJ through multiple mechanisms (Marcand *et al*, 2008). Here, Rap1 binds telomeric DNA directly and its RCT domain engages Rif2 and Sir4 to inhibit end fusions in two parallel pathways. In addition, the central region of Rap1, which harbors the DNA-binding domain but excludes the BRCT and RCT domains, has an independent function in end protection that is only revealed when *rif2* and *sir4* are deleted. In mammalian cells, end protection by Trf2 masks any role of Rap1 under some conditions (Sfeir *et al*, 2010). Protection of chromosome ends by Rap1 is only observed when Trf2 is absent (Sarthy *et al*, 2009) or when cells enter replicative senescence (Lototska *et al*, 2020).

In dissecting the role of Rap1 in end protection, we realized that telomere length profoundly affects end protection. However, in contrast to the long-established view that the shortest telomeres are most at risk of triggering a DNA damage response, we found that long telomeres are also highly vulnerable to end fusions. Rap1 mutants that fully protect wildtype telomeres, fail to prevent fusions of long telomeres. This is observed independently of whether telomere elongation was induced by the deletion of *poz1* or *ppm1* (Figs 5E, and 6C and D), or by using a genetic background with

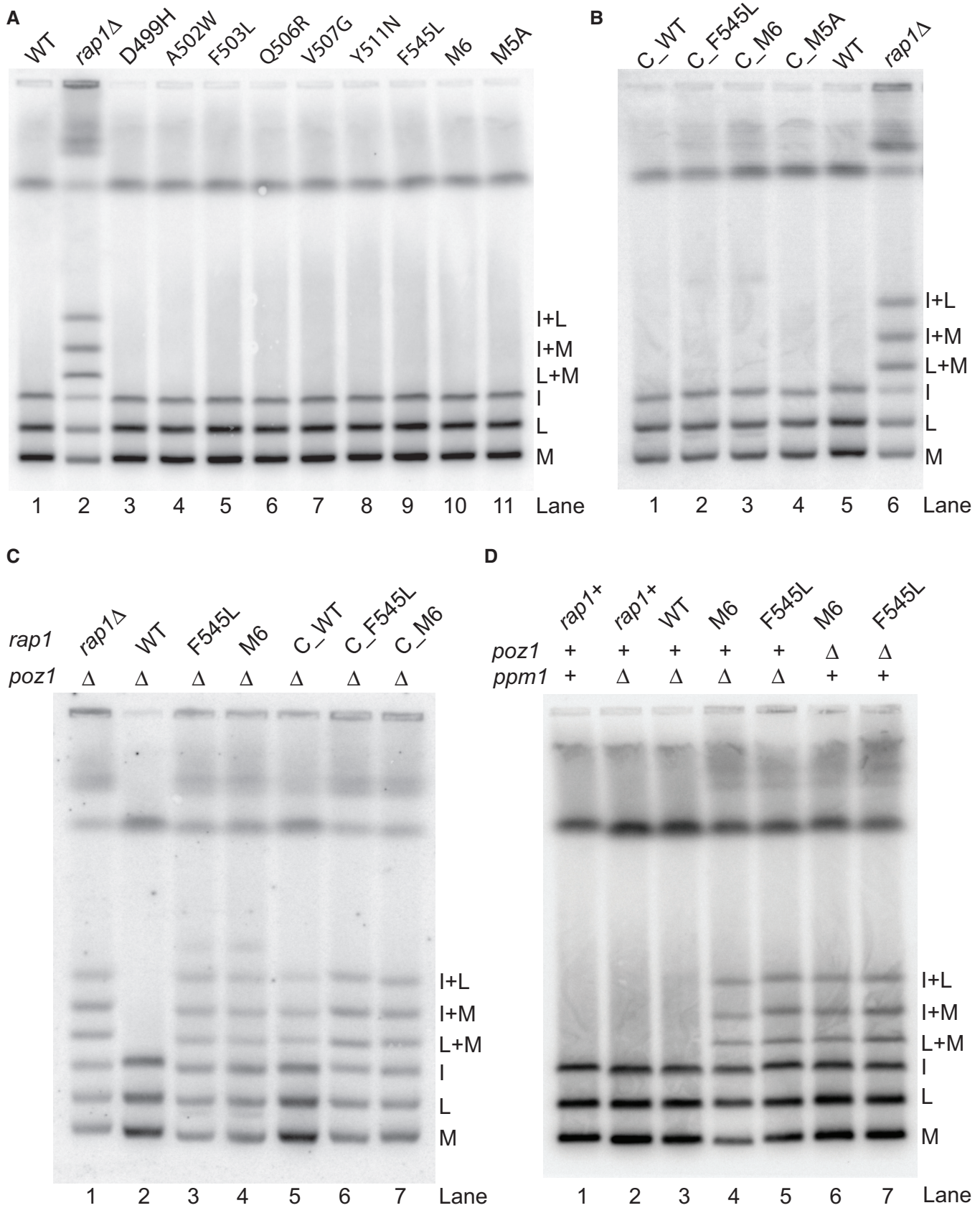

Figure 6.

Figure 6. Rap1 p-patch and F545L mutants fail to protect long telomeres.

A PFGE analysis of nitrogen-starved N-terminally V5-tagged full-length Rap1 mutants. All mutants were integrated at the endogenous *rap1* locus. M5A is the mutation of all 5 nonalanine amino acids under selection in the p-patch to alanine.

B PFGE analysis of nitrogen-starved N-terminally V5-tagged *rap1*_440–693 mutants integrated at the endogenous *rap1* locus.

C PFGE analysis of nitrogen-starved *rap1* mutants in *poz1*Δ background.

D PFGE analysis of nitrogen-starved *rap1* mutants in *ppm1*Δ background. Untagged Rap1 are in lanes 1–2 and N-terminally V5-tagged in lanes 3–7.

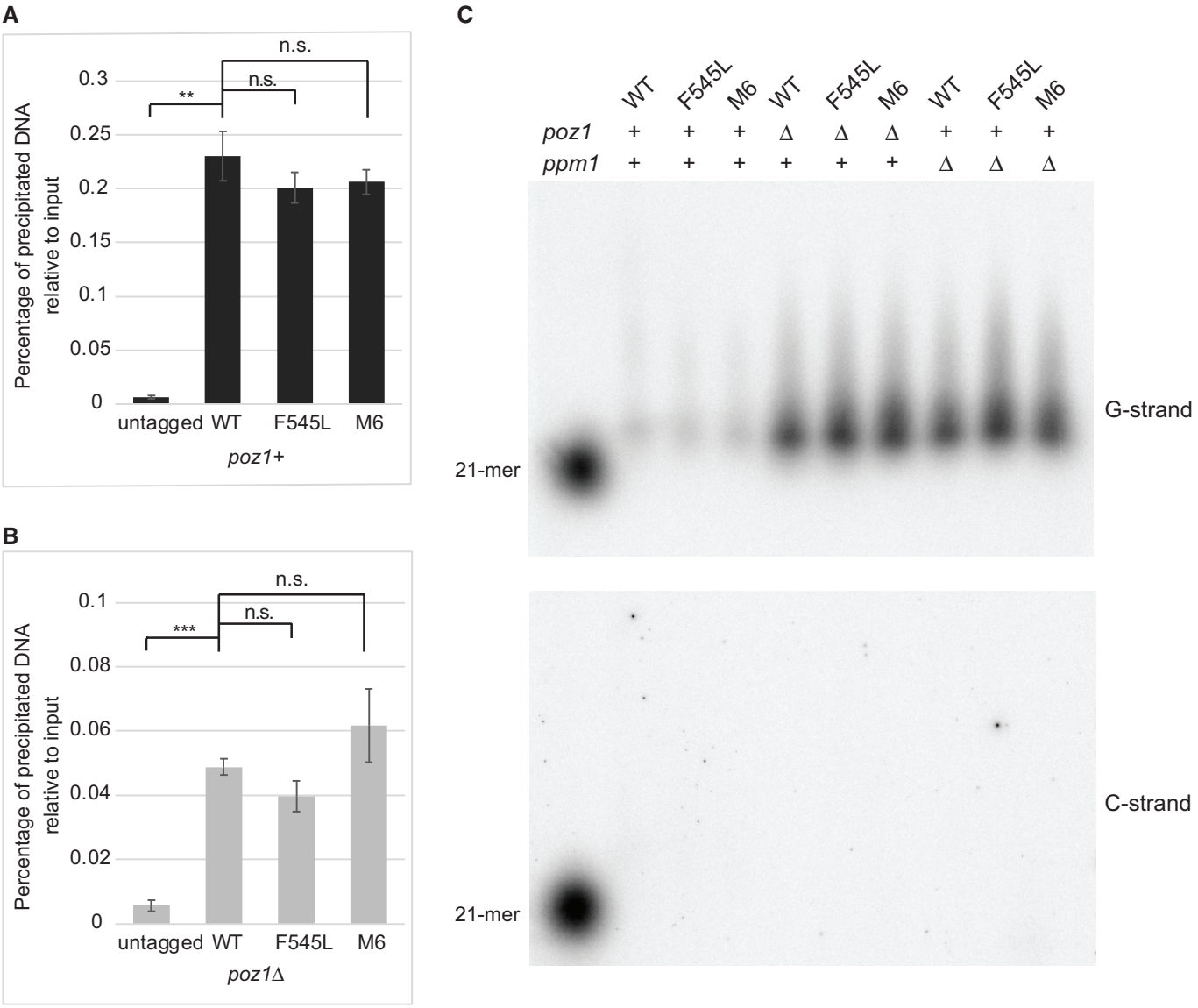

Figure 7. Telomere association and single-stranded overhang analysis.

A ChIP–qPCR analysis of N-terminally V5-tagged WT, F545L, and M6 mutants of Rap1. Untagged Rap1 was used as a control. Bars represent mean of percentage of DNA precipitated with anti-V5 antibody conjugated beads relative to input DNA. Error bars represent SEM. $N = 4$ biological replicates. Two-tailed unpaired Student's *t*-test was performed and significance is indicated. *** $P < 0.001$, ** $0.001 \leq P < 0.01$, n.s.: $P > 0.05$.

B ChIP–qPCR analysis of N-terminally V5-tagged WT, F545L, and M6 mutants of Rap1 in *poz1*Δ background performed as in (A). $N = 4$ biological replicates. Statistical analysis is the same as (A).

C Single-stranded overhang measured by denaturing gel electrophoresis of duplex-specific nuclease digested genomic DNA and Southern blot with oligonucleotide probes specific for the G-strand (top panel) and C-strand (bottom panel). WT, F545L, and M6 mutants of Rap1 in the presence or absence of *poz1* or *ppm1* were analyzed. A 21-mer of $(GGTTACA)_3$ was used as a positive control and size marker for G-strand and a $(TGTAACC)_3$ oligo was used for the C-strand.

Source data are available online for this figure.

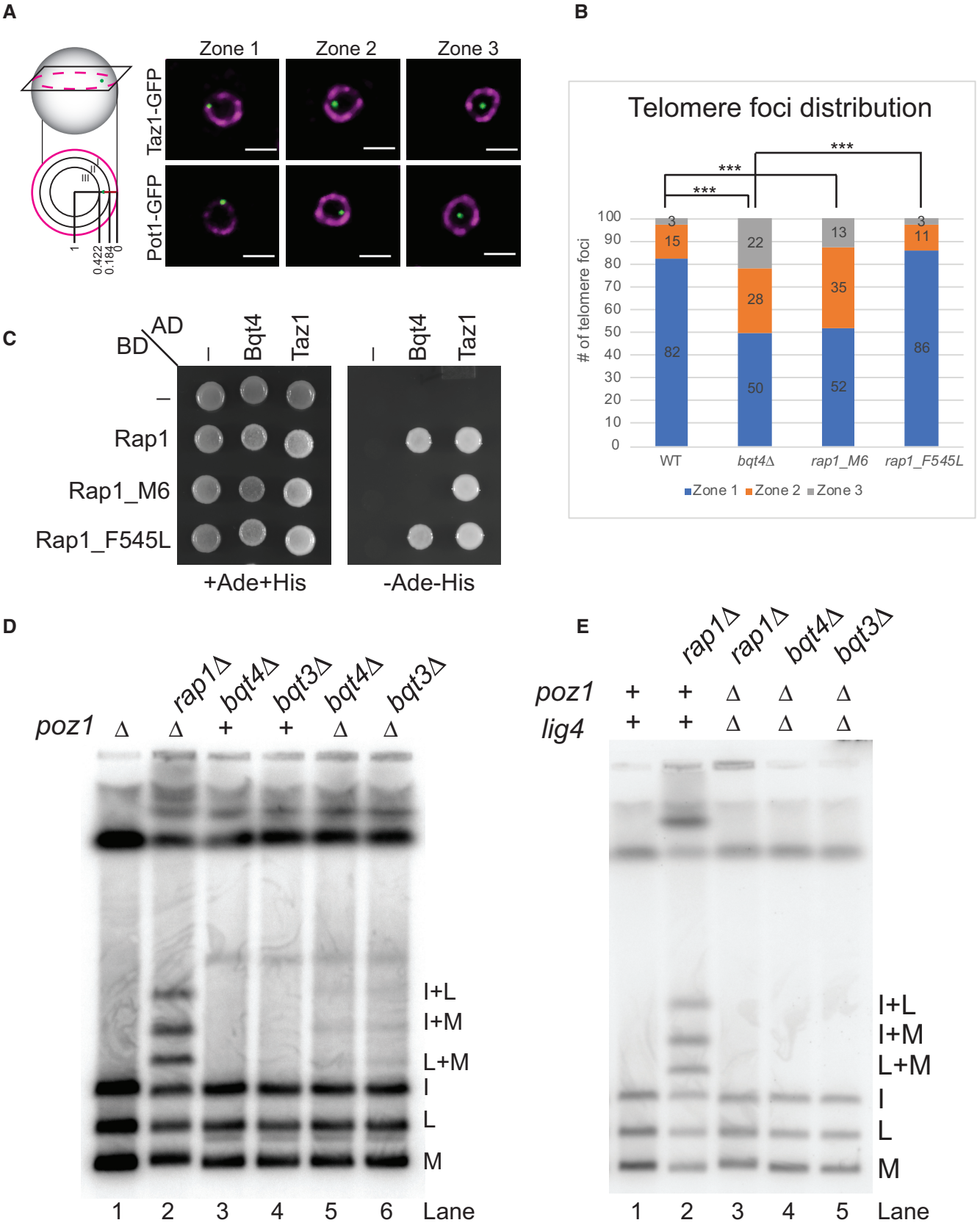

Figure 8.

Figure 8. Nuclear envelope attachment mediates end protection of long telomeres.

A Schematic of scoring matrix. Each nucleus was divided into three concentric zones of equal area with zone I corresponding to the nuclear periphery. The focal plane with the brightest GFP signal and well-defined NE was chosen for measurements. Distance of the GFP spot to NE (X) and diameter of the nucleus were measured for the calculation. GFP signals were allocated to one of the three concentric zones of equal surface area as described (Hediger *et al*, 2002). Zone I: X < 0.184 × radius (r)); Zone II: X between 0.184 and 0.422 times r; and X > 0.422 × r is zone III. Representative images of cells expressing Nup44-mCherry (magenta) and Taz1-GFP or Pot1-GFP (green), respectively. The z-plane showing the brightest GFP spot is shown and was used for quantification. Scale bar: 2 μm.

B Stacking bar chart showing telomere distribution (labeled by Pot1-GFP) in each of the three zones. Hundred telomere foci were quantified per sample. Chi-squared tests were performed by comparing the *rap1* mutants to WT or *bqt4*Δ. Significance is indicated. *** $P < 0.001$.

C Yeast two-hybrid assay probing interaction between Rap1 and Bqt4. WT and mutants of Rap1 were fused to the DNA-binding domain (BD) in pGBKT7. Bqt4 and Taz1 were fused to the Gal4 activation domain (AD) in pGADT7. Cells (5 μl) carrying both plasmids at 5 x 10^6 cells/ml were spotted onto -Leu-Trp dropout plates and -Leu-Trp-Ade-His dropout plates to select for ADE2 and HIS3 markers. "–": Empty BD or AD plasmid.

D PFGE analysis of nitrogen-starved *bqt4*Δ and *bqt3*Δ cells in the presence or absence of *poz1*.

E End fusions in *bqt4*Δ*poz1*Δ and *bqt3*Δ*poz1*Δ are dependent on the presence of ligase IV. PFGE analysis of nitrogen-starved cells in the presence or absence of *lig4*.

Source data are available online for this figure.

initially long telomeres that shortened over time (Figs 2B, and 4B and C).

One explanation for the telomere length dependence of end protection is that elongated telomeres require more telomeric proteins to coat all telomeric repeats. While we cannot exclude the possibility that limiting protein levels provide a partial explanation for our observations, two reasons argue against insufficient Rap1 being responsible for the loss of end protection. Firstly, Rap1 protein is expressed in large excess over what is needed to protect telomeres as demonstrated by its ability to fully protect 10-fold elongated telomeres (Fig 6C and D). Secondly, the protein levels of several mutants were higher than WT, yet they failed to protect against the fusion of elongated telomeres (Figs 5E, and 6C and D), even when telomeres are only slightly longer than wildtype (Fig 5D). Most importantly, Rap1ΔPI and Rap1Δ593–638, two mutants with nonoverlapping deletions, fully inhibit end fusions in the presence of long telomeres, even though Rap1Δ593–638 was expressed at the lowest level of all internal deletion mutants (Fig 1C, and 5B and E). By contrast, the mutations at the positions identified in the screen failed to protect elongated telomeres, strongly indicating a functional significance of the p-patch and F545 in specifically protecting long telomeres.

Mechanistically, the mutations within the p-patch disrupt the tethering of telomeres to the nuclear periphery. Consistent with the loss of this tether rendering long telomeres more vulnerable to undergoing fusions, deletion of *bqt3* or *bqt4* partially phenocopies this sensitivity. Furthermore, TERRA expression and telomere recombination are increased when telomeres detach from the nuclear envelop (Maestroni *et al*, 2020). Similarly, in human cells, telomeres localize to the nuclear periphery during postmitotic nuclear assembly (Crabbe *et al*, 2012) and nuclear envelop tethering has been shown to inhibit the formation of ALT-associated PML bodies and by inference telomere recombination (Yang *et al*, 2021). Another recent study found that telomeres experiencing replication stress due to the presence of the Pot1ΔOB mutant show relocalization of telomeres to the nuclear periphery possibly to preserve telomere integrity (Pinzaru *et al*, 2020). Notably, the presence of Pot1ΔOB in human cells causes extreme telomere lengthening (Loayza & De Lange, 2003) indicating that the presence of a protective mechanism for long telomeres in the nuclear periphery may well be conserved between fission yeast and human cells. By contrast, the localization of telomeres to the nuclear periphery in budding yeast has been proposed to promote genome integrity by stimulating DSB repair of subtelomeric breaks (Therizols *et al*, 2006; Schober *et al*, 2009). However, differences between long and short telomeres were not examined in these studies. It is clear that the tethering of telomeres to the nuclear envelop puts them in a privileged compartment, although the molecular consequences may vary among species and circumstances.

Telomere length is highly heterogenous across evolution, but each species maintains telomeres within a defined size range. This is true even in species with constitutively active telomerase, where shortening of telomeres cannot serve as a tumor suppressive mechanism. It is conceptually easy to see that cells maintain a lower limit of telomere length to preserve the mark that distinguishes a chromosome end from the DNA ends formed by a DNA double-strand break. As telomeres erode past a critical length, a DNA damage response may result in chromosome end fusions, which, in the event of continued cell division, causes genomic rearrangements or mitotic catastrophe (De Lange, 2005; Armanios, 2009; Artandi & DePinho, 2010). By contrast, why cells would maintain an upper limit of telomere length is less clear, even though it has been known for some time that long telomeres pose challenges. Telomeres are fragile sites susceptible to replication fork stalling that require the aid of shelterin components for efficient replication (Miller *et al*, 2006; Sfeir *et al*, 2009). Their G-rich nature also renders telomeres more susceptibility to oxidative damage and longer telomeres are more sensitive to high levels of reactive oxygen species (Rubio *et al*, 2004). Now, our results show that longer telomeres require specific protection against fusions, revealing another challenge for cells with long telomeres to maintain genome integrity. It is thus not surprising that cells have active mechanisms to shorten hyper-elongated telomeres such as telomere rapid deletion events (TRD) or telomere trimming (Li & Lustig, 1996; Wang *et al*, 2004; Pickett *et al*, 2009).

Interestingly, several studies have reported an association between long telomeres and an increased risk for various types of cancer (Lan *et al*, 2009; Lynch *et al*, 2013; Pellatt *et al*, 2013; Julin *et al*, 2015; Machiela *et al*, 2015, 2016, 2017; Ojha *et al*, 2016; Rode *et al*, 2016). The authors' reason that long telomeres provide cells with additional time to accumulate driver mutations while proliferating before short telomeres trigger cell cycle arrest. Our data now suggest an additional but not mutually exclusive explanation: long telomeres may themselves increase genomic instability and thereby drive tumorigenesis.

Materials and Methods

Strains and constructs

All strains used in this study are listed in Appendix Tables S2 and S3. Genomic integrations were generated by one-step gene replacement (Bahler *et al*, 1998). Plasmids used in this study are listed in Appendix Table S4 and were transformed into *S. pombe* by electroporation or into yeast two-hybrid strain AH109 (Takara Bio) according to the manufacturer's manual. Plasmid pLP150 contained *rap1* 440–693 region flanked by 686 base pairs (bp) of the *rap1* endogenous promoter region plus an ATG start codon on the 5′ side and 375 bp of endogenous downstream terminator sequence inserted into pDBlet vector (Brun *et al*, 1995) and was isolated from the mutagenesis library described below. Plasmids pLP161-171 were generated by site-directed mutagenesis using pLP150 as a template.

Telomere length and end fusion analysis

Genomic DNA preparation, telomere length analysis, and pulsed-field gel electrophoresis were carried out following the same procedure as described (Pan *et al*, 2015). Fiji (Schindelin *et al*, 2012) was used for the quantification of Southern blots by comparing combined signal intensities of I + L, I + M, and L + M bands to the total intensity of the I, L, M bands and the three fusion bands.

Denatured protein extract and western blotting

Extract preparation and western blot analysis were carried out as described (Pan *et al*, 2015). Primary antibodies used were mouse anti-V5 (Thermo Fisher Scientific, R960-25) and mouse anti-α-tubulin (Sigma-Aldrich, T5168). HRP-conjugated goat anti-mouse IgG (H + L; Thermo Fisher Scientific, 31430) was used as a secondary antibody.

Mutagenesis library construction and screen

Oligos and DNA templates used for the generation of the mutagenesis library and PCR products for sequencing are listed in Appendix Table S5. Type IIS restriction enzymes were used to avoid the introduction of non-native sequences between the coding region and the promoter and terminator sequences, respectively. First, Rap1 upstream 686 bp and downstream 375 bp regions were amplified by fusion PCR placing two BspMI restriction sites in opposite orientations between the upstream and downstream sequences, followed by cloning into pDblet with SalI and XmaI restriction enzymes to generate pLP143. The resulting plasmid was then digested with BspMI and treated with recombinant shrimp alkaline phosphatase (rSAP) prior to ligation. Rap1 fragment 440 to 693 with added start and stop codons and flanking BmsBI sites was amplified and TOPO-cloned to pCR4-Blunt-TOPO vector (Invitrogen) and sequence verified (pLP142). Random mutagenesis PCR was carried out with GeneMorph II Random Mutagenesis Kit (Agilent) following the manufacturer's instructions with the following specifics: 5.95 ng of pLP142 equivalent to 1 ng of target DNA was used as a template and 30 cycles for PCR. The product was digested with BsmBI and inserted into plasmid pLP143 by ligation. The ligation product was transformed into XL10-gold ultracompetent cells. To preserve the complexity of the library, 12 transformations with 2 µl of ligation reaction per transformation were performed and plated to 73 large (150 mm) plates containing Luria Broth (LB) supplemented with 50 µg/ml carbenicillin. From each plate, ~900 colonies were collected by scraping with a spreader and washing off with LB. Cell pellets were collected by centrifugation at 6,000 × *g* for 15 min and plasmid DNA was isolated using a QIAfilter Plasmid Giga Kit (Qiagen).

The mutagenesis library plasmids were transformed into PP1623A (*rap1*::*natMX*) cells by electroporation. Cells from six transformations with 1 µg of DNA per transformation were pooled after electroporation and allowed to recover in 30 ml YES for 3 h at 32°C. Cells were collected by centrifugation and transferred into 200 ml EMM for overnight culture. Cultures were then diluted to 5×10^5 cells/ml in 400 ml EMM and cultured to mid-log phase ($0.5–1 \times 10^7$ cells/ml). Cells were spun down and washed twice with EMM minus nitrogen (EMM-N), then resuspended in 360 ml EMM-N at 2×10^6 cells/ml, split into three flasks as triplicates (A, B, C), and arrested at 25°C for 48 h. The remaining cells were harvested for genomic DNA isolation as R0 samples. Following arrest, 4×10^8 cells were resuspended in 100 ml EMM for each replicate and recovered for 6 h and then diluted to 5×10^5 cells/ml in 400 ml with EMM and cultured at 32°C overnight. When the cell density reached $0.5–1 \times 10^7$ cells/ml, 2.5×10^8 cells were collected by centrifugation, washed twice with EMM-N, and resuspended in 125 ml EMM-N at 2×10^6 cells/ml for a second round of arrest at 25°C for 48 h. These arrest-recovery cycles were repeated five times. Each round, cells were harvested for PFGE analysis following the arrest and after recovery to mid-log phase, cells were harvested for genomic DNA preparation.

Illumina sequencing and data analysis

Genomic and plasmid DNA from R0 and three replicates of R1 to R5 was isolated as described (Pan *et al*, 2015). To amplify the mutated region for Illumina sequencing, PCR reactions (50 µl) containing 1 × Q5 reaction buffer (NEB), 200 µM dNTPs, 0.5 µM of Bloli6118 and Bloli6119, 1 U of Q5 Hot Start High-Fidelity DNA Polymerase (NEB) and 100 ng genomic DNA from R0-R5 or 93 pg of the original plasmid library isolated from bacteria were incubated at 98°C for 1 min, followed by 18 cycles of 98°C for 10 s, 56°C for 30 s and 72°C for 30 s with a final extension at 72°C for 2 min. PCR products were gel purified with MinElute gel purification kit (Qiagen) and Illumina libraries were prepared with different indexes using Nextera XT Library Prep Kit (Illumina, FC-131-1096). Prior to sequencing, the libraries were pooled at equal molar ratios and spiked in at 3.55% into a pool of unrelated RNA seq libraries to increase the complexity of the sequencing samples and facilitate cluster calling. The libraries were then sequenced using the Illumina HiSeq-2500 platform in rapid mode on a RapidSeq flowcell at 100 bp single read length. The number of reads generated per library is listed in Appendix Table S6.

Sequences were trimmed using Trimmomatic version 0.32 (Bolger *et al*, 2014) as follows: The leading and trailing bases of each read were removed if the quality score was below 3. Reads were scanned 5′ to 3′ with a 4-base window and were clipped when the average quality score dropped below 15. After window clipping and leading/trailing bases were trimmed, reads less than 36 bp long

were dropped. Reads were then aligned to the modified Rap1 sequence using the bwa mem aligner version 0.7.15-r1140 (Li & Durbin, 2009). The resulting alignments were filtered for reads with MAPQ scores greater than or equal to 2, sorted, and then indexed using SAMtools version 1.3.1. Per-position base composition of each alignment was determined using the command line tool pysamstats (https://github.com/alimanfoo/pysamstats; https://github.com/pysam-developers/pysam; Li *et al*, 2009). The resulting tab-separated files were analyzed using Python version 2.7.2 and the data analysis package pandas (McKinney, 2010). Positions in each replicate were selected if the fraction of noncanonical nucleotide decreased from each round of selection to the next. The intersection of these positions was taken across replicates.

Fluorescence microscopy and quantification

Live G1-arrested cells (in EMM-N for 24 h) were mounted on 8-well glass bottom slides (ibidi) coated with concanavalin A and analyzed at 25°C. Fluorescence microscopy images were obtained using a fluorescence spinning disk confocal microscope, VisiScope 5 Elements (Visitron Systems GmbH), which is based on a Ti-2E (Nikon) stand equipped with a spinning disk unit (CSU-W1, 50 µm pinhole, Yokogawa). The set-up was controlled by the VisiView software (Visitron Systems GmbH) and images were acquired with a 100 × oil immersion objective (100 × NA 1.49 lens, Apo SR TIRF) and an sCMOS camera (BSI, Photometrics). Taz1-GFP and Pot1-GFP were detected with a 488 nm excitation laser and ET460/50 emission filter (Chroma). Nup44-mCherry was detected with a 561 nm excitation laser and ET570LP emission filter (Chroma). 3D stacks of images with 14 confocal z-planes at 0.32-µm increments were recorded for each sample. The exposure time was 200 ms for each channel with a live bin of 1.

Fiji was used for image processing and quantification of the telomere foci distribution. Sample identities were blinded for the person performing image acquisition and quantification. In cells with large and well-defined nuclear envelope signals, the focal plane with the brightest GFP signal was chosen for measurements. The diameter of the nuclear envelope and the distance of the GFP spot to the nearest point of the nuclear envelope (X = distance between the center of the spot and center of the NE signal) were measured. GFP signals were allocated to one of the three concentric zones of equal surface area as described (Hediger *et al*, 2002). Zone I ($X < 0.184 \times$ radius (r)) is considered the nuclear periphery. X between 0.184 and 0.422 times r is zone II and $X > 0.422 \times$ r is zone III. For each sample, 100 telomere foci were quantified. Chi-squared tests were performed by comparing the mutants to WT and *bqt4*Δ, respectively.

Chromatin immunoprecipitation (ChIP) assays

Telomere ChIP followed by quantitative real-time PCR analysis was performed as described (Moser *et al*, 2014) with the following modifications and specifications: After lysis, cell lysates were sonicated in bioruptor pico (diagenode) for 5 cycles of 30 s on and 30 s off with cooling. Mouse anti-V5 antibody (Thermo Fisher Scientific, R960-25) was used to pull down V5-tagged Rap1. PCR primers used were jk380 (5'-TATTTCTTTATTCAACTTACCGCACTTC-3′) and jk381 (5'-CAGTAGTGCAGTGTATTATGATAATTAAAATGG-3′) as in (Moser *et al*, 2014). Four biological replicates were performed. Two-tailed unpaired Student's *t*-test was performed for statistical analysis.

Single-stranded overhang length analysis

The single-stranded overhang length was analyzed by adapting the duplex-specific nuclease (DSN) method (Zhao *et al*, 2011). Genomic DNA (1 µg) was digested with 1 U DSN at 37°C for 2 h. The resulting products were subjected to electrophoresis through a 1.2% alkaline agarose gel (50 mM NaOH and 1 mM EDTA) in a cold room at 1.5 V/cm for 18 h. DNA was then transferred by capillary action overnight to the Hybond-XL membrane and UV crosslinked at 70 mJ/cm. Hybridization was performed with ^{32}P-labeled probes in Denhardt's buffer at 42°C overnight and washed two times 15 min with 2x SSC/0.1% SDS and 2 times 15 min with 0.5x SSC/0.1% SDS. The membrane was then exposed to a Phosphorscreen and scanned on an Amersham Typhoon scanner. Oligonucleotide probes $(TGTAACC)_3$ and $(GGTTACA)_3$ were end-labeled with PNK and [γ-^{32}P] ATP and used to probe for G-strand and C-strand, respectively.

Yeast two-hybrid assays

Yeast two-hybrid assays were carried out using pGBKT7 and pGADT7 plasmids and AH109 strain from the Matchmaker system (Takara Bio). Wildtype, M6, and F545L mutants of r*ap1* were cloned into pGBDKT7 plasmid as "baits" and *bqt4* and *taz1* were cloned into pGADT7 plasmid as "preys." The resulting plasmids are listed in Appendix Table S4. pGBKT7 and pGADT7 fusion plasmids were cotransformed into AH109 according to the manufacturer's instructions. ADE2 and HIS3 reporter genes were used for selection. Five microliter of cells at 5×10^6 cells/ml were spotted onto -Leu-Trp dropout media plates and -Leu-Trp-Ade-His dropout plates to select for ADE2 and HIS3 markers.

Data availability

The sequencing data are available in Gene Expression Omnibus (GEO) database with the accession number GSE190759 (https://www.ncbi.nlm.nih.gov/geo/query/acc.cgi?acc=GSE190759). Scripts used in this study are available at https://github.com/baumannlab/Sp_Pan_rap1_select_detect.

Expanded View for this article is available online.

Acknowledgements
We thank Yasushi Hiraoka and Sue Jaspersen for strains, Bettina Moser for advice on ChIP, the Molecular Biology and Media Preparation facilities at the Stowers Institute for Medical Research, and the Media Lab, Microscopy and Genomics Core Facility at the Institute of Molecular Biology for excellent service and support, David V. Ho for computational help, Kristi L. Jensen for comments on the manuscript and all members of the Baumann laboratory for helpful discussions. This work was supported in part by the Deutsche Forschungsgemeinschaft (DFG; German Research Foundation; project number 393547839 – SFB 1361, sub-project 17), the Max Planck Graduate Center with the Johannes Gutenberg University Mainz, the Howard Hughes Medical

Institute, and the Stowers Institute for Medical Research. P.B. is an Alexander von Humboldt Professor at Johannes Gutenberg University.

Author contributions

Peter Baumann: Conceptualization; formal analysis; supervision; funding acquisition; methodology; writing – review and editing. **Lili Pan:** Formal analysis; investigation; methodology; writing – original draft. **Duncan Tormey:** Software; formal analysis. **Nadine Bobon:** Formal analysis; investigation.

Disclosure and competing interests statement

The authors declare that they have no conflict of interest.

References

Armanios M (2009) Syndromes of telomere shortening. *Annu Rev Genomics Hum Genet* 10: 45 – 61

Artandi SE, DePinho RA (2010) Telomeres and telomerase in cancer. *Carcinogenesis* 31: 9 – 18

Bae NS, Baumann P (2007) A RAP1/TRF2 complex inhibits nonhomologous end-joining at human telomeric DNA ends. *Mol Cell* 26: 323 – 334

Bahler J, Wu JQ, Longtine MS, Shah NG, McKenzie A III, Steever AB, Wach A, Philippsen P, Pringle JR (1998) Heterologous modules for efficient and versatile PCR-based gene targeting in *Schizosaccharomyces pombe*. *Yeast* 14: 943 – 951

Baumann P, Cech TR (2001) Pot1, the putative telomere end-binding protein in fission yeast and humans. *Science* 292: 1171 – 1175

Bilaud T, Brun C, Ancelin K, Koering CE, Laroche T, Gilson E (1997) Telomeric localization of TRF2, a novel human telobox protein. *Nat Genet* 17: 236 – 239

Bolger AM, Lohse M, Usadel B (2014) Trimmomatic: a flexible trimmer for Illumina sequence data. *Bioinformatics* 30: 2114 – 2120

Broccoli D, Smogorzewska A, Chong L, de Lange T (1997) Human telomeres contain two distinct Myb-related proteins, TRF1 and TRF2. *Nat Genet* 17: 231 – 235

Brun C, Dubey DD, Huberman JA (1995) pDblet, a stable autonomously replicating shuttle vector for *Schizosaccharomyces pombe*. *Gene* 164: 173 – 177

Chen Y, Rai R, Zhou ZR, Kanoh J, Ribeyre C, Yang Y, Zheng H, Damay P, Wang F, Tsujii H *et al* (2011) A conserved motif within RAP1 has diversified roles in telomere protection and regulation in different organisms. *Nat Struct Mol Biol* 18: 213 – 221

Chikashige Y, Hiraoka Y (2001) Telomere binding of the Rap1 protein is required for meiosis in fission yeast. *Curr Biol* 11: 1618 – 1623

Chikashige Y, Yamane M, Okamasa K, Tsutsumi C, Kojidani T, Sato M, Haraguchi T, Hiraoka Y (2009) Membrane proteins Bqt3 and −4 anchor telomeres to the nuclear envelope to ensure chromosomal bouquet formation. *J Cell Biol* 187: 413 – 427

Chong L, van Steensel B, Broccoli D, Erdjument-Bromage H, Hanish J, Tempst P, de Lange T (1995) A human telomeric protein. *Science* 270: 1663 – 1667

Collopy LC, Ware TL, Goncalves T, í Kongsstovu S, Yang Q, Amelina H, Pinder C, Alenazi A, Moiseeva V, Pearson SR *et al* (2018) LARP7 family proteins have conserved function in telomerase assembly. *Nat Commun* 9: 557

Cooper JP, Nimmo ER, Allshire RC, Cech TR (1997) Regulation of telomere length and function by a Myb-domain protein in fission yeast. *Nature* 385: 744 – 747

Crabbe L, Cesare AJ, Kasuboski JM, Fitzpatrick JA, Karlseder J (2012) Human telomeres are tethered to the nuclear envelope during postmitotic nuclear assembly. *Cell Rep* 2: 1521 – 1529

De Lange T (2005) Telomere-related genome instability in cancer. *Cold Spring Harb Symp Quant Biol* 70: 197 – 204

de Lange T (2018) Shelterin-mediated telomere protection. *Annu Rev Genet* 52: 223 – 247

Ferreira MG, Cooper JP (2001) The fission yeast Taz1 protein protects chromosomes from Ku-dependent end-to-end fusions. *Mol Cell* 7: 55 – 63

Fujita I, Nishihara Y, Tanaka M, Tsujii H, Chikashige Y, Watanabe Y, Saito M, Ishikawa F, Hiraoka Y, Kanoh J (2012a) Telomere-nuclear envelope dissociation promoted by Rap1 phosphorylation ensures faithful chromosome segregation. *Curr Biol* 22: 1932 – 1937

Fujita I, Tanaka M, Kanoh J (2012b) Identification of the functional domains of the telomere protein Rap1 in *Schizosaccharomyces pombe*. *PLoS ONE* 7: e49151

Hediger F, Neumann FR, Van Houwe G, Dubrana K, Gasser SM (2002) Live imaging of telomeres: yKu and sir proteins define redundant telomere-anchoring pathways in yeast. *Curr Biol* 12: 2076 – 2089

Houghtaling BR, Cuttonaro L, Chang W, Smith S (2004) A dynamic molecular link between the telomere length regulator TRF1 and the chromosome end protector TRF2. *Curr Biol* 14: 1621 – 1631

Hu C, Inoue H, Sun W, Takeshita Y, Huang Y, Xu Y, Kanoh J, Chen Y (2019) Structural insights into chromosome attachment to the nuclear envelope by an inner nuclear membrane protein Bqt4 in fission yeast. *Nucleic Acids Res* 47: 1573 – 1584

Julin B, Shui I, Heaphy CM, Joshu CE, Meeker AK, Giovannucci E, De Vivo I, Platz EA (2015) Circulating leukocyte telomere length and risk of overall and aggressive prostate cancer. *Br J Cancer* 112: 769 – 776

Kanoh J, Ishikawa F (2001) spRap1 and spRif1, recruited to telomeres by Taz1, are essential for telomere function in fission yeast. *Curr Biol* 11: 1624 – 1630

Kim JK, Liu J, Hu X, Yu C, Roskamp K, Sankaran B, Huang L, Komives EA, Qiao F (2017) Structural basis for Shelterin bridge assembly. *Mol Cell* 68: 698 – 714

Kim SH, Kaminker P, Campisi J (1999) TIN2, a new regulator of telomere length in human cells. *Nat Genet* 23: 405 – 412

Lan Q, Cawthon R, Shen M, Weinstein SJ, Virtamo J, Lim U, Hosgood HD III, Albanes D, Rothman N (2009) A prospective study of telomere length measured by monochrome multiplex quantitative PCR and risk of non-Hodgkin lymphoma. *Clin Cancer Res* 15: 7429 – 7433

Li B, Lustig AJ (1996) A novel mechanism for telomere size control in *Saccharomyces cerevisiae*. *Genes Dev* 10: 1310 – 1326

Li B, Oestreich S, de Lange T (2000) Identification of human Rap1: Implications for telomere evolution. *Cell* 101: 471 – 483

Li H, Durbin R (2009) Fast and accurate short read alignment with burrows-wheeler transform. *Bioinformatics* 25: 1754 – 1760

Li H, Handsaker B, Wysoker A, Fennell T, Ruan J, Homer N, Marth G, Abecasis G, Durbin R (2009) The sequence alignment/map format and SAMtools. *Bioinformatics* 25: 2078 – 2079

Liu D, Safari A, O'Connor MS, Chan DW, Laegeler A, Qin J, Songyang Z (2004) PTOP interacts with POT1 and regulates its localization to telomeres. *Nat Cell Biol* 6: 673 – 680

Loayza D, De Lange T (2003) POT1 as a terminal transducer of TRF1 telomere length control. *Nature* 423: 1013 – 1018

Lorenzi LE, Bah A, Wischnewski H, Shchepachev V, Soneson C, Santagostino M, Azzalin CM (2015) Fission yeast Cactin restricts telomere transcription and elongation by controlling Rap1 levels. *EMBO J* 34: 115 – 129

Lototska L, Yue JX, Li J, Giraud-Panis MJ, Songyang Z, Royle NJ, Liti G, Ye J, Gilson E, Mendez-Bermudez A (2020) Human RAP1 specifically protects telomeres of senescent cells from DNA damage. *EMBO Rep* 21: e49076

Lynch SM, Major JM, Cawthon R, Weinstein SJ, Virtamo J, Lan Q, Rothman N, Albanes D, Stolzenberg-Solomon RZ (2013) A prospective analysis of telomere length and pancreatic cancer in the alpha-tocopherol beta-carotene cancer (ATBC) prevention study. *Int J Cancer* 133: 2672 – 2680

Machiela MJ, Hofmann JN, Carreras-Torres R, Brown KM, Johansson M, Wang Z, Foll M, Li P, Rothman N, Savage SA *et al* (2017) Genetic variants related to longer telomere length are associated with increased risk of renal cell carcinoma. *Eur Urol* 72: 747 – 754

Machiela MJ, Hsiung CA, Shu XO, Seow WJ, Wang Z, Matsuo K, Hong YC, Seow A, Wu C, Hosgood HD III *et al* (2015) Genetic variants associated with longer telomere length are associated with increased lung cancer risk among never-smoking women in Asia: A report from the female lung cancer consortium in Asia. *Int J Cancer* 137: 311 – 319

Machiela MJ, Lan Q, Slager SL, Vermeulen RC, Teras LR, Camp NJ, Cerhan JR, Spinelli JJ, Wang SS, Nieters A *et al* (2016) Genetically predicted longer telomere length is associated with increased risk of B-cell lymphoma subtypes. *Hum Mol Genet* 25: 1663 – 1676

Maciejowski J, Li Y, Bosco N, Campbell PJ, de Lange T (2015) Chromothripsis and Kataegis induced by telomere crisis. *Cell* 163: 1641 – 1654

Maestroni L, Reyes C, Vaurs M, Gachet Y, Tournier S, Geli V, Coulon S (2020) Nuclear envelope attachment of telomeres limits TERRA and telomeric rearrangements in quiescent fission yeast cells. *Nucleic Acids Res* 48: 3029 – 3041

Marcand S, Pardo B, Gratias A, Cahun S, Callebaut I (2008) Multiple pathways inhibit NHEJ at telomeres. *Genes Dev* 22: 1153 – 1158

McKinney W (2010) Data structures for statistical computing in python. In *Proceedings of the 9th Python in Science Conference*, Millman S.v.d.W.a.J. (ed.), pp. 51 – 56. https://conference.scipy.org/proceedings/scipy2010/pdfs/mckinney.pdf

Mennie AK, Moser BA, Nakamura TM (2018) LARP7-like protein Pof8 regulates telomerase assembly and poly(a)+TERRA expression in fission yeast. *Nat Commun* 9: 586

Miller KM, Ferreira MG, Cooper JP (2005) Taz1, Rap1 and Rif1 act both interdependently and independently to maintain telomeres. *EMBO J* 24: 3128 – 3135

Miller KM, Rog O, Cooper JP (2006) Semi-conservative DNA replication through telomeres requires Taz1. *Nature* 440: 824 – 828

Miyoshi T, Kanoh J, Saito M, Ishikawa F (2008) Fission yeast Pot1-Tpp1 protects telomeres and regulates telomere length. *Science* 320: 1341 – 1344

Moretti P, Freeman K, Coodly L, Shore D (1994) Evidence that a complex of SIR proteins interacts with the silencer and telomere-binding protein RAP1. *Genes Dev* 8: 2257 – 2269

Moser BA, Chang YT, Nakamura TM (2014) Telomere regulation during the cell cycle in fission yeast. *Methods Mol Biol* 1170: 411 – 424

Ojha J, Codd V, Nelson CP, Samani NJ, Smirnov IV, Madsen NR, Hansen HM, de Smith AJ, Bracci PM, Wiencke JK *et al* (2016) Genetic variation associated with longer telomere length increases risk of chronic lymphocytic leukemia. *Cancer Epidemiol Biomarkers Prev* 25: 1043 – 1049

Paez-Moscoso DJ, Pan L, Sigauke RF, Schroeder MR, Tang W, Baumann P (2018) Pof8 is a La-related protein and a constitutive component of telomerase in fission yeast. *Nat Commun* 9: 587

Pan L, Hildebrand K, Stutz C, Thoma N, Baumann P (2015) Minishelterins separate telomere length regulation and end protection in fission yeast. *Genes Dev* 29: 1164 – 1174

Pardo B, Marcand S (2005) Rap1 prevents telomere fusions by nonhomologous end joining. *EMBO J* 24: 3117 – 3127

Pellatt AJ, Wolff RK, Torres-Mejia G, John EM, Herrick JS, Lundgreen A, Baumgartner KB, Giuliano AR, Hines LM, Fejerman L *et al* (2013) Telomere length, telomere-related genes, and breast cancer risk: the breast cancer health disparities study. *Genes Chromosomes Cancer* 52: 595 – 609

Pfeiffer V, Lingner J (2013) Replication of telomeres and the regulation of telomerase. *Cold Spring Harb Perspect Biol* 5: a010405

Pickett HA, Cesare AJ, Johnston RL, Neumann AA, Reddel RR (2009) Control of telomere length by a trimming mechanism that involves generation of t-circles. *EMBO J* 28: 799 – 809

Pinzaru AM, Kareh M, Lamm N, Lazzerini-Denchi E, Cesare AJ, Sfeir A (2020) Replication stress conferred by POT1 dysfunction promotes telomere relocalization to the nuclear pore. *Genes Dev* 34: 1619 – 1636

Rode L, Nordestgaard BG, Bojesen SE (2016) Long telomeres and cancer risk among 95 568 individuals from the general population. *Int J Epidemiol* 45: 1634 – 1643

Rubio MA, Davalos AR, Campisi J (2004) Telomere length mediates the effects of telomerase on the cellular response to genotoxic stress. *Exp Cell Res* 298: 17 – 27

Sarthy J, Bae NS, Scrafford J, Baumann P (2009) Human RAP1 inhibits non-homologous end joining at telomeres. *EMBO J* 28: 3390 – 3399

Schindelin J, Arganda-Carreras I, Frise E, Kaynig V, Longair M, Pietzsch T, Preibisch S, Rueden C, Saalfeld S, Schmid B *et al* (2012) Fiji: An open-source platform for biological-image analysis. *Nat Methods* 9: 676 – 682

Schober H, Ferreira H, Kalck V, Gehlen LR, Gasser SM (2009) Yeast telomerase and the SUN domain protein Mps3 anchor telomeres and repress subtelomeric recombination. *Genes Dev* 23: 928 – 938

Sfeir A, Kabir S, van Overbeek M, Celli GB, de Lange T (2010) Loss of Rap1 induces telomere recombination in the absence of NHEJ or a DNA damage signal. *Science* 327: 1657 – 1661

Sfeir A, Kosiyatrakul ST, Hockemeyer D, MacRae SL, Karlseder J, Schildkraut CL, de Lange T (2009) Mammalian telomeres resemble fragile sites and require TRF1 for efficient replication. *Cell* 138: 90 – 103

Sievers F, Wilm A, Dineen D, Gibson TJ, Karplus K, Li W, Lopez R, McWilliam H, Remmert M, Soding J *et al* (2011) Fast, scalable generation of high-quality protein multiple sequence alignments using Clustal omega. *Mol Syst Biol* 7: 539

Therizols P, Fairhead C, Cabal GG, Genovesio A, Olivo-Marin JC, Dujon B, Fabre E (2006) Telomere tethering at the nuclear periphery is essential for efficient DNA double strand break repair in subtelomeric region. *J Cell Biol* 172: 189 – 199

Wang RC, Smogorzewska A, de Lange T (2004) Homologous recombination generates T-loop-sized deletions at human telomeres. *Cell* 119: 355 – 368

Yang CW, Hsieh MH, Sun HJ, Teng SC (2021) Nuclear envelope tethering inhibits the formation of ALT-associated PML bodies in ALT cells. *Aging (Albany NY)* 13: 10490 – 10516

Ye JZ, Hockemeyer D, Krutchinsky AN, Loayza D, Hooper SM, Chait BT, de Lange T (2004) POT1-interacting protein PIP1: a telomere length regulator that recruits POT1 to the TIN2/TRF1 complex. *Genes Dev* 18: 1649 – 1654

Zhao Y, Shay JW, Wright WE (2011) Telomere G-overhang length measurement method 1: the DSN method. *Methods Mol Biol* 735: 47 – 54

Zhong Z, Shiue L, Kaplan S, de Lange T (1992) A mammalian factor that binds telomeric TTAGGG repeats in vitro. *Mol Cell Biol* 12: 4834 – 4843